Remote sensing of american maple in alluvial forests: a case study in an island complex of the Loire valley (France)

Hilaire Martin [1],
Jean-Matthieu Monnet [2],
Marie De Boisvilliers [3],
Richard Chevalier [1],
Marc Villar [4]

Due to their particular topographic position between land and river, riparian forests are ecosystems rich in biodiversity. In France, along the Middle Loire (from Nevers to Angers), Black poplar (*Populus nigra* L.) forests are often in mixtures with the American maple (*Acer negundo* L.), introduced into the country in the 18th century. We tested the detectability of American maple by LiDAR and very high-resolution multispectral imagery on an island complex. We found that coupling the point cloud height standard deviation with a vegetation index in the red, green and blue spectrums discriminated American maple with a success rate of more than 90%.

Keywords: *Acer negundo*, American Maple, Box Elder, *Populus nigra*, Black Poplar, Airborne Laser Scanning, Remote Sensing, Exogenous Woody Species, Loire River

Introduction

Riparian forests are a key component of river ecosystems due to their position at the interface between water and land (Naiman et al. 2005, Gurnell 2014). In the ana-branch river landscape of the Middle Loire in France (around 400 km between Nevers and Angers), alluvial forests represent a significant part of the vegetation biomass (Grivel & Gautier 2012). Because of their vulnerability to anthropomorphic impact (Rodrigues et al. 2006), riparian forests are considered to be habitats of Special Community Interest in the Habitats Directive 92/43/CEE (EUNIS: G1.11 – Beslin & Gazeau 2016). In these habitats, groundwater reduction due to channel digging (Dunford et al. 2009), water pollution and the introduction of exogenous woody species have perturbed the natural colonization by *Salicaceae* of river banks and islands (Asner et al. 2008). For example, the American maple (*Acer negundo* L., AC) was introduced in France in 1732 (Dumas 2019) and is now commonly found in native Black poplar (*Populus nigra* L., PN) stands (Berg et al. 2017). In addition, the reintroduction of the European beaver in the 1970's indirectly favored colonization by the introduced species since beaver consumes the Black poplar but not the American maple.

In view of the above-mentioned elements, regular monitoring of riparian forests is important for their conservation and management, all the more so in a context of global warming, as these forests vary with the water level from one year to another and present multiple aspects. Thus, mapping these alluvial forests and updating the maps on a near-annual basis are the most appropriate tools to ensure quality monitoring. Currently, cartography has made tremendous progress thanks to Geographic Information Systems (GIS) software and satellite or aerial imagery (Dufour et al. 2013, Huylenbroeck et al. 2020). In France, the National Forest Inventory carries out a permanent inventory of forest resources and provides a great deal of data, including interactive maps. Data are collected at both the stand and tree levels. At the stand level, the forest cover type is in- terpreted from infrared aerial images at a 50-cm resolution. The final product is a vector layer (BD Foret V2) with polygons of 0.5 ha minimum attributed to 32 categories of species composition. However, neither AC nor PN has a category of its own, so this data cannot be used to monitor their spatial dynamics. At the tree level, many parameters are recorded on the NFI sample plots in different scientific domains such as dendrometry, botany and pedology (Hervé et al. 2014). Tree data include diameter, species and position, and height for a sub sample. However, precise plot locations are not publicly available, which prevents cross-analysis with external geographical data. Furthermore, plot density is 1 plot/ 2km² with surveys only every 5 years, thus making the data unsuitable for statistical analysis of small areas.

Aerial imagery provides only two-dimensional images that do not enable direct measurement of the vertical components of the forest canopy. However, in the beginning of the twenty-first century, technological advances in drones and active remote sensing, in particular through the development of new sensors, opened promising perspectives for accessing forest structures (Campbell et al. 2017). For instance, UAVs (Unmanned Aerial Vehicles) with Light Detection and Ranging (LiDAR) provide a three-dimensional geo-referenced point cloud corresponding to the surface objects that intercept the laser pulses from a scanner mounted on an aircraft (Balenović et al. 2013). Though the first uses of LiDAR were mainly devoted to digital terrain models (Wehr & Lohr 1999), numerous applications in forestry have since been investigated.

An overview of the bibliography reveals that there are two main approaches to tree crown delineation from LiDAR data. The

Fig. 1 - Study area. The Mareau-aux-prés islands are located within the large National Natural Reserve of Saint-Mesmin, downstream from Orléans (Loiret, France).
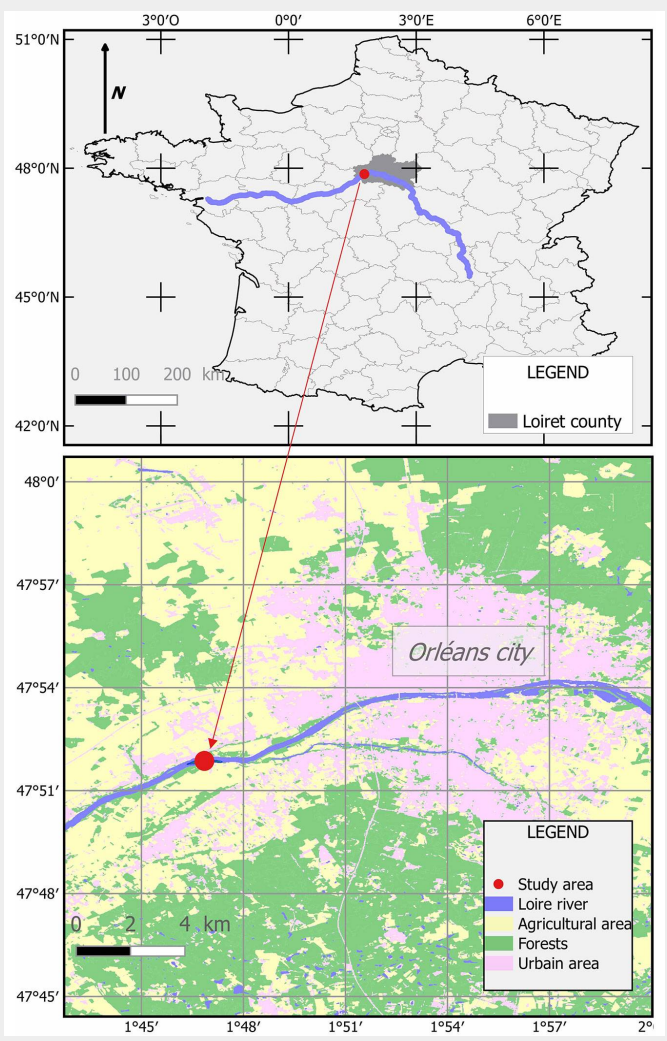
Reserve along the Loire River. We focused on the use of open-source software tools with visual interpretation for training and validation steps to ensure that the method could be applied to larger areas.

Material and methods

Study area

The research was conducted in central France in the Loiret county, on the Mareau-aux-Prés islands in the Loire River (within the boundaries of the Saint-Mesmin National Nature Reserve) near the village of Mareau-aux-Prés (Fig. 1), approximately 10 km downstream from the city of Orléans (47° 51′ 51.88″ N, 01° 46′ 52.84″ E). The total area of the experiment was about 10 ha and elevation ranged from 84 to 89 m a.s.l. The mosaic of four islands (Fig. 2) is mainly dominated by species from the Salicaceae family – adult black poplar and willow shrubs (*Salix* spp.) – except for the central island (C) where, in September 2012, the vegetation was uprooted and the island was leveled and lowered in order to maintain the flow capacity of the Loire river and to prevent floods. A new sedimentary bar appeared in spring 2013 and was colonized by Black poplar and willow seedlings; this island was therefore surveyed with the three other islands.

Image and LiDAR acquisition

Because terns were nesting on the banks, we were allowed to fly over the islands only after August 15. The UAV flights were carried out on 20 and 21 August 2017 by "*L'Avion Jaune*", a French aerial mapping operator using an octorotor FOX-C8 Onyxstar®. The level of the Loire River was one meter above zero, corresponding to summer low water. Eight successive flights occurred; three with a LiDAR sensor, then five others with a camera. LiDAR data were acquired by a YellowScan Surveyor® (YellowScan, Montferrier-sur-Lez, France), which included an onboard computer controlling three main components: a Velodyne laser scanner (VLP16), a Global Navigation Satellite System (GNSS) and an Inertial Navigation System (INS) built by Applanix (APX15). The flight height for the LiDAR was 45 m with a line spacing of 45 m and a sidelap of 60%. The average point density per m² was 215. Multispectral imagery was acquired with a mapping system conceived by *L'Avion Jaune*. The latter con-

first one aims to model tree shape directly in the LiDAR cloud, but this process is quite complex (Monnet 2011, Jaafar et al. 2018). The second approach involves reducing the LiDAR cloud from 3D to 2D. This simplification is interesting because rasters have a longer development history than other approaches (Monnet et al. 2010, Zhen et al. 2016). The 3D-to-2D approach relies on the detection of treetops in the canopy height model (CHM). Then, the crowns are delineated with the watershed algorithm, which reverses the image and considers the crown envelope as a basin (Mei & Durrieu 2004, Lindberg & Holmgren 2017). To ensure proper delineation of the trees, the algorithm's parameters must be carefully chosen in order to correspond to tree

allometries, which are often species- and structure-specific. Applying watershed theory to the forest requires some intrinsic parameters for tree architecture, such as the distance to the nearest treetop, crown size, etc.

Our main goal was to test the ability of the various parameters in the tree segmentation function of the "lidaRtRee" package (Monnet 2018) running on free R software to predict American maple stands in Black poplar island forests. Another objective of this technical paper is to assess the ability of combined LiDAR data and multispectral data acquired by unmanned aerial vehicles (UAVs) to distinguish American maple from Black poplar at the tree level. The test site was located in a French National Nature
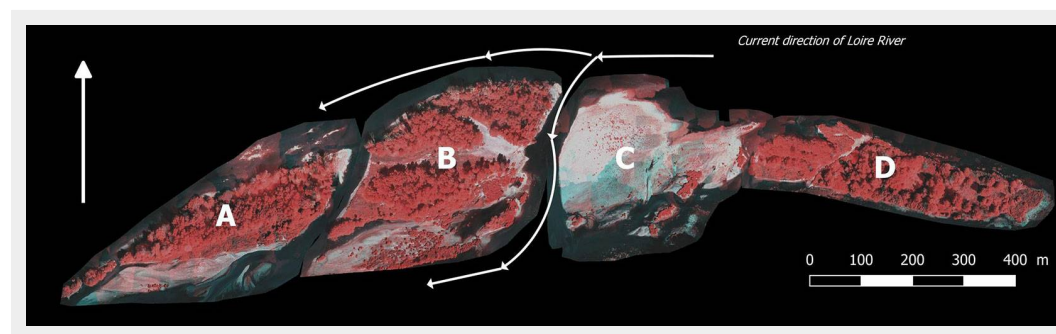
Fig. 2 - The mosaic of four islands. Letters indicate the name of the islands.

sisted of a pair of identical digital single-lens reflex cameras (Canon® EOS 500D) – one modified to assess the near infrared (NIR) wavelength, while the other unmodified camera assessed the visible wavelengths (RGB). The flight height for multispectral acquisition was 100 m with a side-lap of 60% and a frontlap of 80%.

Workflow

The workflow was divided into three main steps (Fig. 3): (i) data pre-processing; (ii) tree crown delineation; (iii) model classification.

Data pre-processing: LiDAR data

Raw data processing was done by the mapping operator. LiDAR data were processed by successively running them through the PosPAC software by Applanix, a Surveyor QGIS plugin by YellowScan, and TerraMatch and TerraScan modules by TerraSolid. The classified point cloud was delivered in LAS format. The Digital Terrain Model (DTM) and the Canopy Height Model (CHM) were delivered in Geotif format at 0.2-m resolution. In order to compare different tree segmentations, we created a flood and non-flood forest mask within the mosaic of islands (Fig. 4.). Since American maple mainly colonizes river banks (Gurnell 2014), we excluded the hardwood forest (oak, elm, ash), located on higher terrain (in the non-flood area on island B), and retained only values between 0 and 2.5 m in height. This general mask was applied to all image treatments, including point clouds, DTM and CHM files, and orthophotos.

Data pre-processing: multispectral imagery and vegetation index

Multispectral imagery processing was performed according to scripts developed by *L'Avion Jaune* and the Correlator3D soft-
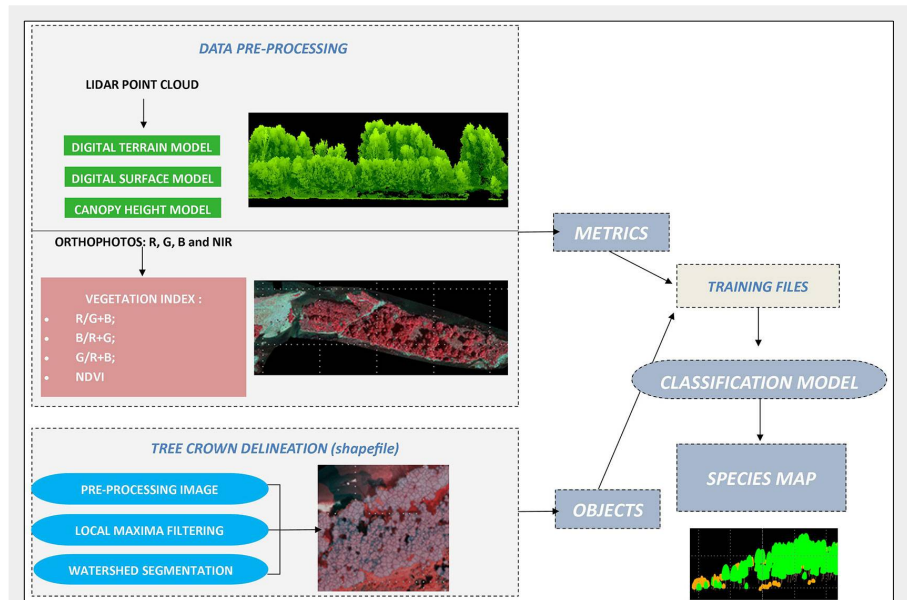

Fig. 3 - Workflow.

ware by Simactive. An orthophoto with four spectral bands (blue, green, red and near-infrared) was generated with a Ground Sample Distance (GSD) of 0.02 m. The orthophoto was resampled to 0.2 m for consistency with the CHM.

Then four simple vegetation indices, excluding the infrared wavelength, were computed: (i) Red / (Green + Blue); (ii) Green / (Red + Blue); (iii) Blue / (Green + Red). We also computed the (iv) Normalized Difference Vegetation Index (NDVI – Rouse et al. 1973).

Tree crown delineation

This step is important because it determines the location and extent of the crowns. Subsequently, the data extracted

inside the delineated crowns are used to select the discrimination variables in the classification step. Tree segmentation was performed with the "treeSegmentation" function from the "lidaRtRee" package (Monnet 2018) of the R software (R Development Core Team 2017). Delineation was based on a 3-phase approach, with each phase requiring several values for parametrization.

First, we applied filters to remove noise from the CHM file. A "salt-and-pepper" noise generally appears when there are CHM pixels with no corresponding laser points (due to the shading effect of trees, for example), or when there is a low number of pixels inside the canopy. The low and zero values were removed by applying

Fig. 4 - Canopy Height Model with non-riparian hardwood forest excluded.
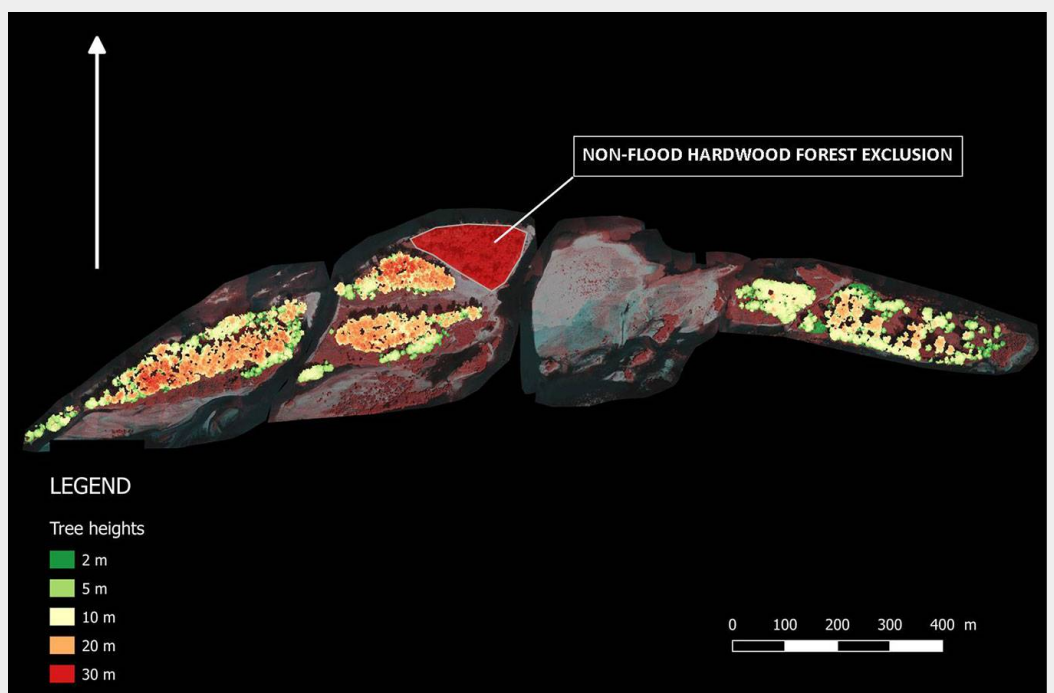
Tab. 1 - Parameters of the "treeSegmentation" function ("lidaRtRee" package). (*): Variables tested and their range of values.

Name	Function
nFilter, nlSize	Prevents "salt and pepper" where no laser points are recorded. We used the default option "Closing" and 3 for size.
sigma *	Prevents branches in a crown from being considered as trees. We tested from 0.1 to 0.9
dmin/dprop	Treetop minimum distance to the next higher pixel and distance as a proportion of height to the next higher pixel. We set these two values at "0" due to crown overlap
hmin	Minimum treetop height: 3 m due to tall nettles
crownProp *	Minimum height of tree crown as a proportion of treetop height. We tested from 0.1 to 0.9
crownMinH	Minimum crown height. We set this value at 3 m.

a closing filter on a 3-pixel-wide neighborhood, which is the default parameter. We next applied a Gaussian filter to smooth out small local variations; this prevents multiple branches from being detected as separate apices (Monnet 2011). Smoothing intensity is driven by the sigma value of the Gaussian filter, which must be adapted to the tree structure and species. In our study, we tested all values from 0.1 to 0.9.

The second step was to select maximum tree height. We first set a minimum treetop height parameter with a value of 3 m in order to avoid confusion with local maxima related to herbs and shrubs. For example, in summer 2017, nettles (*Urtica* sp.) reached as much as 2.5 m in height. We then used horizontal neighborhood parameters to take into account the minimum distance between one maximum treetop height and nearby crowns of the same height. Considering the important overlap between crowns in the forest, no selection based on minimum distance was applied (*i.e.*, a minimum distance of zero was applied).

The third step was tree crown delineation. To segment the crown extension, we applied a marked-based watershed algorithm. Segments in watershed analysis are delineated by selecting local maxima as the start points of watersheds created by flooding a model surface; this process reverses the CHM. Each local maximum has its corresponding crown (segment). In order to exclude neighboring shrubs from the crown segment, two operations were performed: (i) pixels lower than 3 m were excluded from the crowns; (ii) inside each crown, we further excluded the pixels lower than the crown proportion multiplied by treetop height. The resulting parameter reflects the ratio between crown depth and tree height, and must be adapted depending on stand structure. We tested all values between 0.1 (the tree crown extended almost to the ground) and 0.9 (the crown was located within the highest 10% of the tree).

The different parameters tested and their values are listed in Tab. 1.

Classification model: reference data

In order to build a model capable of separating *Acer negundo* (AC) and *Populus nigra* (PN), a reference dataset was created by using the 0.02 cm resolution orthophotos. Very high resolution imagery, such as provided by UAV, are ideal for photointerpretation (Huylenbroeck et al. 2020). The operator selected a total of 316 disks of 1 m diameter and classified them as AC (157) or PN (159). Although the operator is both a botanist and an experienced GIS operator with exhaustive field knowledge of the study site, classification errors might be present in this reference dataset.

Classification model: variables tested

In order to classify the two tree species, variables were computed for each delineated crown based on the CHM, the point cloud and the orthophoto intersecting the crown segments. Tab. 2 presents the variables tested sorted by category: tree metrics (T), LiDAR metrics (L) and orthophoto indices (O). We tested different combinations: (i) T + L + O; (ii) T + L; (iii) L + O; (iv) T + O; (v) T; (vi) L; (vii) O. This made seven possible combinations mixed with nine

Tab. 2 - Metrics computed.

Metrics group	Metrics	Description
Tree metrics (T)	s	Crown surface
	v	Crown volume
	chm.sd	Height standard deviation
	zskew	Skewness of height distribution
	zkurt	Kurtosis of height distribution
	zentropy	Normalized Shannon diversity index of height distribution
LiDAR metrics (L)	zpcum1	Cumulative percentage of return in the 1st layer
	zpcum2	Cumulative percentage of return in the 2nd layer
	zpcum3	Cumulative percentage of return in the 3rd layer
	zpcum4	Cumulative percentage of return in the 4th layer
	zpcum5	Cumulative percentage of return in the 5th layer
	zpcum6	Cumulative percentage of return in the 6th layer
	zpcum7	Cumulative percentage of return in the 7th layer
	zpcum8	Cumulative percentage of return in the 8th layer
	zpcum9	Cumulative percentage of return in the 9th layer
	isd	Standard deviation of intensity
	iskew	Skewness of intensity distribution
	ikurt	Kurtosis of intensity distribution
	ipcumzq10	Percentage of intensity returned below the 10th percentile of height
	ipcumzq30	Percentage of intensity returned below the 30th percentile of height
	ipcumzq50	Percentage of intensity returned below the 50th percentile of height
	ipcumzq70	Percentage of intensity returned below the 70th percentile of height
	ipcumzq90	Percentage of intensity returned below the 90th percentile of height
Orthophoto Indices (O)	m.r.gb	Median (R/(G+B))
	m.g.rb	Median (B/(R+G))
	m.b.rg	Median (B/(R+G))
	m.ndvi	Median (NDVI)
	sd.r.gb	Standard deviation of (R/(G+B))
	sd.g.rb	Standard deviation of (B/(R+G))
	sd.b.rg	Standard deviation of (B/(R+G))
	sd.ndvi	Standard deviation of (NDVI)

Fig. 5 - Overall accuracy (% on the y-axis) of the metrics groups tested (on the x-axis) according to crown proportion (values in gray horizontal) and Gaussian filter (values in gray vertical). Metrics groups tested were: Tree metrics (T), LiDAR metrics (L) and Orthophotos indices (O). Combinations tested were: T+L+O, T+L, L+O, T+O, T, L, O. White rectangles correspond to the number of trees used for training and validation. Green dots correspond to an accuracy > 94%.
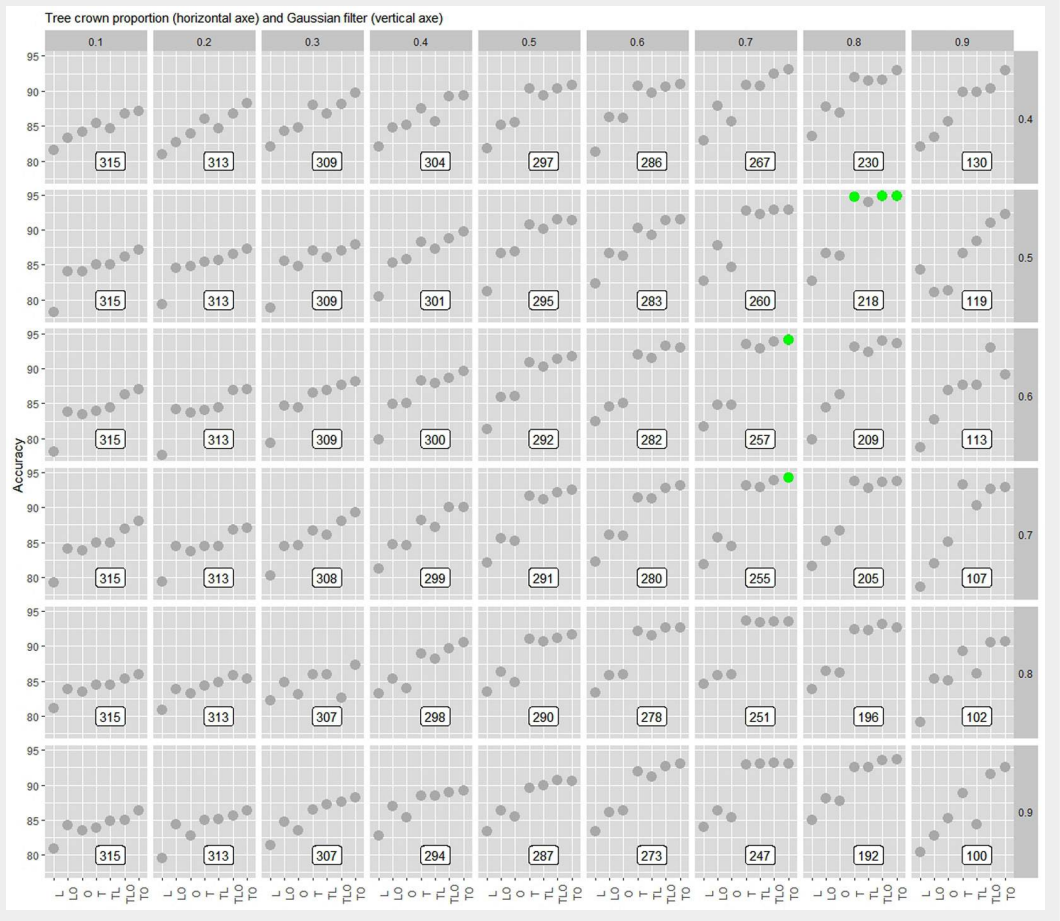
possibilities for the Gaussian filter and nine possibilities for the crown proportion (567 processes).

Direct height variables such as CHM, DTM and point cloud minimum, mean or maximum values were *a priori* discarded from the analysis, based on our knowledge of fluvial dynamics. Indeed, local island topography changes annually due to sand accretion and erosion. Therefore, keeping a fixed height topography value set on the Mareau-aux-Prés complex would have falsified our extrapolation for the Middle-Loire stretch of the river. Secondly, due to the propagation strategy of the American maple, whose seeds arrive by cohort on exposed river banks (Straigyte et al. 2015), a classification based on height values might have merely reflected the age difference between PN and AC, particularly at our study location in the National Reserve. This would also have led to erroneous extrapolated results for other areas along the Loire River.

Classification model: decision tree

In order to select discriminating variables, we used Decision Tree in the R party package (Hothorn et al. 2006). To confirm our results, we ran each decision tree 250 times.

Results

The entire classification process was run on the riparian forests of the Mareau-aux-

Prés islands (Islands: A, B and D – Fig. 4), excluding the hardwood forests. We tested 567 processes and report their overall accuracy and standard deviation in Tab. S1 (Supplementary material).

The accuracy of our classification varied with Gaussian filter and with crown proportion according to metrics group. In Fig. 5, we only present the results from Gaussian filter 0.4 because below this threshold, none of the models succeeded (see Tab. S1 in Supplementary material). Best overall accuracy is represented by green dots for a value greater than 94%. These results concerned all of the metrics groups since the best combinations were: T, TLO, and TO with crown proportions from 0.7 to 0.8 and Gaussian filters from 0.5 to 0.7. To select the best metrics groups, we had to take into account the number of trees used for training/validation. Indeed, as shown in Fig. 5, we observed that the more the
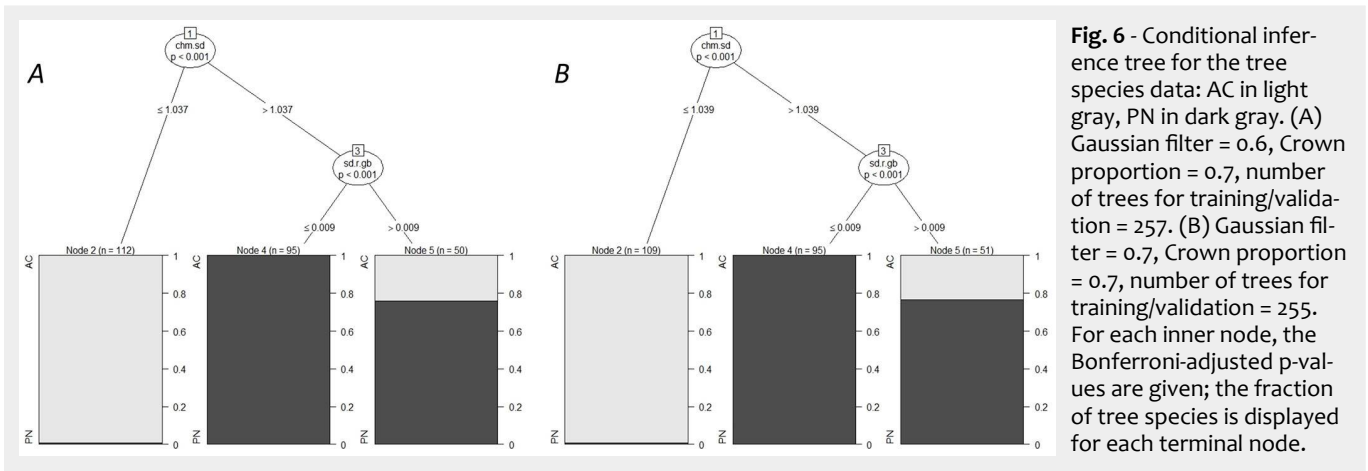
crown proportion and the Gaussian filter increased, the more the number of trees decreased. We then found the best compromise between the best precision and the largest number of trees for training/validation (out of a total of 316 trees selected by visual interpretation). Tab. 3 shows the results of the green dot values and their standard deviations in Fig. 5. We observed that overall accuracy and standard deviations were close and that the number of trees used for training/validation was actually relevant. Finally, we opted for Gaussian filter values of 0.7 and 0.6, and for a crown proportion value of 0.7.

Fig. 6 shows that, for both values of Gaussian filter (A and B), point cloud height standard deviation was the most robust discriminating variable to distinguish AC from PN. Indeed, even below a height value of just one meter, we consistently detected AC. Above this threshold, a vege-

Tab. 3 - Overall accuracy assessment (mean ± standard deviation of 250 repetitions) and number of trees in the reference dataset for the metrics groups selected according to the tree segmentation parameters. (T/V): training / validation; (T): tree metrics; (L): LiDAR metrics; (O): Ortophotos indices.

Gaussian filter	crownProp	T/V tree number	TLO	TO	T
0.7	0.7	255	-	94.3 ± 2.7	-
0.6	0.7	257	-	94.1 ± 2.5	-
0.5	0.8	219	94.8 ± 2.5	94.8 ± 2.4	94.7 ± 2.3

Fig. 6 - Conditional inference tree for the tree species data: AC in light gray, PN in dark gray. (A) Gaussian filter = 0.6, Crown proportion = 0.7, number of trees for training/validation = 257. (B) Gaussian filter = 0.7, Crown proportion = 0.7, number of trees for training/validation = 255. For each inner node, the Bonferroni-adjusted p-values are given; the fraction of tree species is displayed for each terminal node.

tation index Red / (Green + Blue) standard deviation below 0.009 discriminated PN. However, above 0.009 there was an uncertainty of more than 20% for the prediction of PN.

Fig. 7 presents a prediction map showing that American maple is mainly confined to the outer edges of the islands.

Discussion

Our results show that, within the National Nature Reserve of Mareau-aux-Prés, point cloud height standard deviation and the standard vegetation index Red / (Green + Blue) predict the presence of American maple (*Acer negundo* L.) in more than 90% of the riparian Black poplar (*Populus nigra* L.) forests.

The retained variables correspond respectively to the groups of tree metrics (point cloud height standard deviation) and the orthophoto indices (standard vegetation index).

In the context of introduced species in al-luvial forest contexts, our results reinforce the use of LiDAR coupled with photogrammetry (Manfreda et al. 2018, Huylenbroeck et al. 2020), although comparison with previous research also displays differences. In a Mediterranean riparian forest, Dunford et al. (2009) distinguished five classes including four tree species with an overall accuracy of 91% from a single RGB image of 13 cm resolution obtained from UAV. Their reference data consisted of homogeneous terrain units identified on the field with an inclusive sampling and then digitized on the imagery. The overall accuracy dropped to 71% at the mosaic scale, partly because of radiometry differences in images. The greater accuracy achieved in our case might be explained by the height information added by LiDAR data, as well as the lower number of classes. The radiometry issue might be a problem when analysing larger areas which would require more images and acquisition time with a UAV. With bi-spectral LiDAR data, Laslier et al. (2019)

classified eight species of a riparian forest in Normandy (France) with an overall accuracy of 67%. Their study also highlights the importance of elevation metrics for classification. Intensity-related metrics did not bring much improvement in their classification, suggesting that spectral information of LiDAR might not be as straigthforward to use as with imagery. Differences with our results might be explained in part by the fact that they explored a larger gradient of tree species, while we limited ourselves to two species. A wider variety of species can present complex internal canopy structures revealed by LiDAR metrics. When comparing the importance of variables from multispectral and hyperspectral imagery and full-wave form LiDAR for the classification of four tree species in a temperate forest, Heinzel & Koch (2012) found out that the NIR channel had great importance. Height metrics derived from LiDAR were not selected, but there was one LiDAR metric linked with the internal struc-
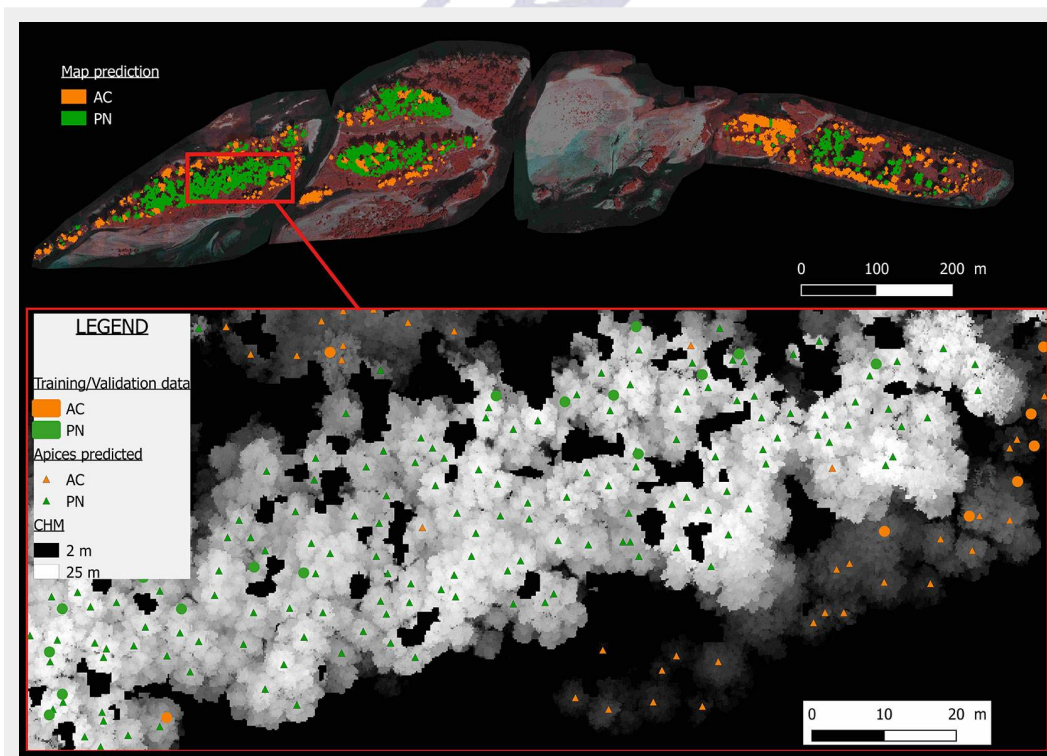
Fig. 7 - Prediction map. Upper part of the figure: prediction map of the American maple (AC, in orange) and Black poplar (PN, in green). Lower part of the figure: an example on a part of the furthest island from the study: circles represent the data interpreted visually, triangles represent the predicted apices, symbology of colors is identical to that previously described.

ture. Differences with our findings might be due to the fact that they considered both deciduous and coniferous species, which have different reflectance in NIR. Dalponte et al. (2012) showed that LiDAR height metrics improved the classification of mountainous forests into seven tree species compared to multispectral data only. The variability in findings available in the literature shows that depending on species and forest structures, and probably on acquisition period, there are variations in the importance of metrics of different types for species classification.

The results obtained here are rather encouraging regarding the potential for mapping AN dynamics on larger areas with simple variables. Meanwhile, we must be aware of limitations as pointed out by Huylenbroeck et al. (2020) regarding upscaling of results. In the case of longer stretch of river, the relevance of spectral indices might decrease because of issues with radiometric calibration of images and greater variability of forest species, structure and phenology. The use of reference data based only on photointerpretation might also introduce bias or error in the training and validation processes, but it makes also possible to build larger datasets by taking advantage of very high resolution imagery available from UAV. It is clear that this step is highly dependent both on the operator's experience in visual interpretation and his knowledge of the study area, but it is essential to calibrate the predictions as well as possible (Manfreda et al. 2018, Demarchi et al. 2020). The trade-off between variability representation thanks to sample size and noise due to visual interpretation still has to be investigated in order to design cost-efficient operational protocols for the acquisition of reference data for species mapping in larger areas.

However, there are limitations to our findings, especially for Black poplar. Indeed, our results do not take into account an indirect beaver-consumption effect. By consuming Black poplar, the beaver generates holes in the canopy that allow the LiDAR to better penetrate the crowns at the tree scale. If we were to extend our work to all of the Middle-Loire from Nevers to Angers (a distance of about 400 km), the results would be at least partially dependent on beaver population density per linear kilometer. How accurate would our classification model be without the presence of the beaver?

One way to solve this problem would be to repeat overflights and test the crown delineation function with tree shape settings. This method was tested on Belgium riparian forests by Michez et al. (2016). Although the image analyses differ according to our study accuracy is greatly increased by repeated overflights. More overflights would likely improve detectability for American maple under the canopy of the taller Black poplars.

Lastly, as Pirotti et al. (2017) show in their study, we could also test other tree crown delineation algorithms such as "Li 2012" and "Dalponte 2016". The Dalponte 2016 algorithm (Dalponte & Coomes 2016) is similar to the one we used in this study since it starts from rather similar parameters and then segments the CHM. On the other hand, Li's 2012 algorithm (Li et al. 2012) does not use a CHM and works directly on the point cloud instead. Though algorithms based directly on the point cloud seem to take more processing time, they could enable researchers to explore the canopy structure of these Loire-island forests.

Conclusion

American maple (*Acer negundo* L.) is an introduced species, which competes with the endemic Black poplar (*Populus nigra* L.). We used an airborne LiDAR scanner and imagery-derived vegetation index data to discriminate American maple from Black poplar with 90% accuracy on a complex of four islands inside the National Nature Reserve of Saint-Mesmin in the Loire River (France), based on a training and validation dataset obtained by photointerpretation. Mapping the American maple is all the more important since beavers (reintroduced in the 1970s) do not consume it, though it consumes Black poplar. We found that tree crown delineation is optimized by the "treeSegmentation" function from the "lidaRtRee" package (Monnet 2018) running under free R software (R Development Core Team 2017). We tested two important parameters of this function: the Gaussian filter and crown proportion. The first parameter prevents big branches in a crown being considered as trees. The second optimizes the proportion of the crown relative to the total height. We found that the best values for the Gaussian filter and crown proportion were respectively 0.7 (and 0.6) and 0.7. We also found that the best predictors were point cloud height standard deviation and the standard deviation of a simple vegetation index based on RGB wavelengths, Red/ (Green + Blue).

Acknowledgements

References

Asner GP, Knapp DE, Kennedy-Bowdoin T, Jones MO, Martin RE, Boardman J, Hughes RF (2008). Remote sensing of native and invasive species in Hawaiian forests. Remote Sensing of Environment 112: 1942-1945. - doi: 10.1016/j.rse.2007.11.016

Balenović I, Alberti G, Marjanović H (2013). Airborne laser scanning - the status and perspectives for the application in the South-East European forestry. South-East European Forestry 4 (2): 59-79. - doi: 10.15177/seefor.13-07

Berg C, Drescher A, Essl F (2017). Using relevé-based metrics to explain invasion patterns of alien trees in temperate forests. Tuexenia 37: 127-142. [online] URL: http://d-nb.info/1151140155/34

Beslin O, Gazeau J-C (2016). Système d'Information des Évolutions du Lit de la Loire et de ses affluents. Typologie des habitats du SIEL 2. Guide de terrain et de lecture pour la cartographie [Information System of the Evolutions of the Loire riverbed and its tributaries. SIEL Habitat Typology 2. Field and Reading Guide for Mapping]. Conservatoire National du Bassin Parisien, délégation Centre-Val de Loire, Orléans, France, pp. 1-27. [in French]

Campbell L, Coops N, Saunders S (2017). LiDAR as an advanced remote sensing technology to augment ecosystem classification and mapping. Journal of Ecosystems and Management 17 (1): 1-13. [online] URL: http://jem-online.org/forrex/index.php/jem/article/view/588

Dalponte M, Bruzzone L, Gianelle D (2012). Tree species classification in the Southern Alps based on the fusion of very high geometrical resolution multispectral/hyperspectral images and LiDAR data. Remote Sensing of Environment 123: 258-270. - doi: 10.1016/j.rse.2012.03.013

Dalponte M, Coomes DA (2016). Tree-centric mapping of forest carbon density from airborne laser scanning and hyperspectral data. Methods in Ecology and Evolution 7: 1236-1245. - doi: 10.1111/2041-210X.12575

Demarchi L, Kania A, Ciezkowski W, Piórkowski H, Oswiecimska-Piasko Z, Chormanski J (2020). Recursive feature elimination and random forest classification of Natura 2000 grasslands in lowland river valleys of Poland based on airborne hyperspectral and LiDAR data fusion. Remote Sensing 12: 1-33. - doi: 10.3390/rs12111842

Dufour S, Bernez I, Betbeder J, Corgne S, Hubert-Moy L, Nabucet J, Rapinel S, Sawtschuk J, Trollé C (2013). Monitoring restored riparian vegetation: how can recent developments in remote sensing sciences help? Knowledge and Management of Aquatic Ecosystems 410 (10): 1-15. - doi: 10.1051/kmae/2013068

Dumas Y (2019). Que savons-nous de l'Erable négondo (Acer negundo L., 1753)? [What do we know about American maple (*Acer negundo* L., 1753)?]. Naturae (10): 257-283.

Dunford R, Michel K, Gagnage M, Piégay H, Trémelo M-L (2009). Potential and constraints of unmanned aerial vehicle technology for the characterization of Mediterranean riparian forest. International Journal of Remote Sensing 30

(19): 4915-4935. - doi: 10.1080/01431160903023025

Grivel S, Gautier E (2012). Mise en place des îles fluviales en Loire moyenne, du 19e siècle à aujourd'hui [Establishment of fluvial islands in the middle Loire, from the 19th century to today]. Cybergeo, European Journal of Geography, Document no. 615. [in French] - doi: 10.4000/cybergeo.25451

Gurnell A (2014). Plants as river system engineers. Earth Surface Processes and Landforms 39 (1): 4-25. - doi: 10.1002/esp.v39.1

Heinzel J, Koch B (2012). Investigating multiple data sources for tree species classification in temperate forest and use for single tree delineation. International Journal of Applied Earth Observation and Geoinformation 18: 101-110. - doi: 10.1016/j.jag.2012.01.025

Hervé J-C, Wurpillot S, Vidal C, Roman-Amat B (2014). L'inventaire des ressources forestières en France: un nouveau regard sur de nouvelles forêts [Inventory of forest resources in France: a new look at new forests]. Revue Forestière Française 66 (3): 247-260. [in French] - doi: 10.4267/2042/56055

Hothorn T, Hornik K, Zeileis A (2006). Unbiased recursive partitioning: a conditional inference framework. Journal of Computational and Graphical Statistics 15 (3): 651-674. - doi: 10.1198/106186006X133933

Huylenbroeck L, Laslier M, Dufour S, Georges B, Lejeune P, Adrien M (2020). Using remote sensing to characterize riparian vegetation: a review of available tools and perspectives for managers. Journal of Environmental Management 267: 1-19. - doi: 10.1016/j.jenvman.2020.110652

Jaafar WSWM, Woodhouse IH, Silva CA, Omar H, Abdul Maulud KN, Hudak AT, Klauberg C, Cardil A, Mohan M (2018). Improving individual tree crown delineation and attributes estimation of tropical forests using airborne LiDAR data. Forests 9 (12): 1-23. - doi: 10.3390/f9120759

Laslier M, Hubert-Moy L, Dufour S (2019). Mapping riparian vegetation functions using 3D bispectral LiDAR data. Water 11 (3): 483. - doi: 10.3390/w11030483

Lindberg E, Holmgren J (2017). Individual tree crown methods for 3D data from remote sensing. Current Forestry Report 3: 19-31. - doi: 10.1007/s40725-017-0051-6

Li W, Guo Q, Jakubowski MK, Kelly M (2012). A new method for segmenting individual trees from the lidar point cloud. Photogrammetric Engineering and Remote Sensing 78: 75-84. - doi: 10.14358/PERS.78.1.75

Manfreda S, McCabe MF, Miller PE, Lucas R, Pajuelo Madrigal V, Mallinis G, Ben Dor E, Helman D, Estes L, Ciraolo G, Müllerová J, Tauro F, De Lima MI, De Lima JLMP, Maltese A, Frances F, Caylor K, Kohv M, Perks M, Ruiz-Pérez G, Su Z, Vico G, Toth B (2018). On the use of unmanned aerial systems for environmental monitoring. Remote Sensing 10: 1-33. - doi: 10.3390/rs10040641

Mei C, Durrieu S (2004). Tree crown delineation from digital elevation models and high resolution imagery. In: Proceedings of the ISPRS Working Group part 8/2. Freiburg (Germany) 3-6 Oct 2004. The International Archives of the Photogrammetry, Remote Sensing, vol. 36, pp. 6. [online] URL: http://www.researchgate.net/publication/228986087

Michez A, Piégay H, Lisien J, Claessens H, Lejeune P (2016). Classification on riparian forest species and health condition using muti-temporal and hyperspatial imagery from unmanned aerial system. Environmental Monitoring and Assessment 188 (146): 1-19.

Monnet J-M, Mermin E, Chanussot J, Berger F (2010). Tree top detection using local maxima filtering: a parameter sensitivity analysis. In: Proceedings of "Silvilaser 2010 - 10th International Conference on LIDAR Applications for Assessing Forest Ecosystems". Freiburg (Germany) 14 Sep 2010, pp. 9. [online] URL: http://hal.archives-ouvertes.fr/hal-00523245/

Monnet J-M (2011). Caractérisation des forêts de montagne par scanner laser aéroporté: estimation de paramètres de peuplement par régression SVM et apprentissage non supervisé pour la détection de sommets [Using airborne laser scanning for mountain forests mapping: Support vector regression for stands parameters estimation and unsupervised training for treetop detection]. PhD thesis, Grenoble Images Parole Signal Automatique Department, Université de Grenoble Alpes, France, pp. 187. [online] URL: http://www.theses.fr/2011GRENT056

Monnet J-M (2018). lidaRtRee, forest analysis with airborne laser scanning (Lidar) data. Web site. [online] URL: http://gitlab.irstea.fr/jean-matthieu.monnet/lidaRtRee

Naiman RB, Décamps H, McClain ME (2005). Riparia: ecology, conservation, and management of streamside communities. Elsevier Academic Press, London, UK, pp. 418.

Pirotti F, Kobal M, Roussel J-R (2017). A comparison of tree segmentation methods using very high density airborne laser scanner data. International Archives of the Photogrammetry, Remote Sensing and Spatial Information Sciences XLII-2/W7: 285-290. - doi: 10.5194/isprs-archives-XLII-2-W7-285-2017

R Development Core Team (2017). R: a language and environment for statistical computing. R Foundation for Statistical Computing, Vienna. [online] URL: http://www.r-project.org/

Rodrigues S, Bréhéret J-G, Macaire J-J, Greulich S, Villar M (2006). In-channel woody vegetation controls on sedimentary processes and the sedimentary record within alluvial environments: a modern example of an anabranch of the River Loire, France. Sedimentology 54 (1): 223-242. - doi: 10.1111/j.1365-3091.2006.00832.x

Rouse J, Haas RH, Schell JA, Deering DW (1973). Monitoring vegetation systems in the great plains with ERTS. In: Proceeding of the "3rd ERTS Symposium". Washington (DC, USA) 10-14 Dec 1973. NASA SP-351 1, US Government Printing Office, Washington, DC, USA, pp. 309-317.

Straigyte L, Cekstere G, Laivins M, Marozas V (2015). The spread, intensity and invasiveness of the *Acer negundo* in Riga and Kaunas. Dendrobiology 74: 157-168. - doi: 10.12657/denbio.074.016

Wehr A, Lohr U (1999). Airborne laser scanning an introduction and overview. ISPRS Journal of Photogrammetry and Remote Sensing 54: 68-82. - doi: 10.1016/S0924-2716(99)00011-8

Zhen Z, Quackenbush L, Zhang L (2016). Trends in automatic individual tree crown detection and delineation evolution of LiDAR data. Remote Sensing 8 (4): 333. - doi: 10.3390/rs8040333

Supplementary Material

Tab. S1 - Overall accuracy (%) and standard deviation of the metrics groups tested according to crown proportion and Gaussian filter.

Link: Martin_3237@suppl001.pdf